ACS OMEGA

http://pubs.acs.org/journal/acsodf

Article

Ratiometric Fluorescent Biosensor Based on Forster Resonance Energy Transfer between Carbon Dots and Acridine Orange for miRNA Analysis

Zhiwei Sun,[▽] Yao Tong,[▽] Xiaoyu Zhou, Juan Li, Li Zhao, Hui Li, Chuanxin Wang, Lutao Du,* and Yanyan Jiang*

Cite This: *ACS Omega* 2021, 6, 34150−34159

Read Online

ACCESS | Metrics & More | Article Recommendations | Supporting Information

ABSTRACT: The expression level of miRNA is highly correlated with the pathological process of malignant tumors. Therefore, the abnormal expression of miRNA in serum is considered as reliable evidence for the existence of tumor cells. Here, a ratiometric fluorescent biosensor based on the Forster resonance energy transfer between fluorophores is proposed for detecting colorectal cancer-specific miRNA (miR-92a-3p). The miRNA in serum was first isolated by carboxyl-modified SiO_2 microspheres. Then, the addition of miRNA to the detection system resulted in the distance change between the donor acridine orange (AO) and the acceptor fluorescent carbon dots (CDs), which made the fluorescence signal change. The physicochemical properties, especially the fluorescence characteristics of CDs and AO, which enabled the ratiometric fluorescence detection, were comprehensively studied. The ratiometric fluorescent biosensor could detect miRNA in the concentration range of 1−9 nM and showed a detection limit of 0.14 nM. Moreover, the ratiometric fluorescent biosensor exhibited high selectivity for the target miRNA. The validity of the ratiometric fluorescent biosensor was also verified using the serum sample, demonstrating its potential for enzyme-free miRNA analysis.

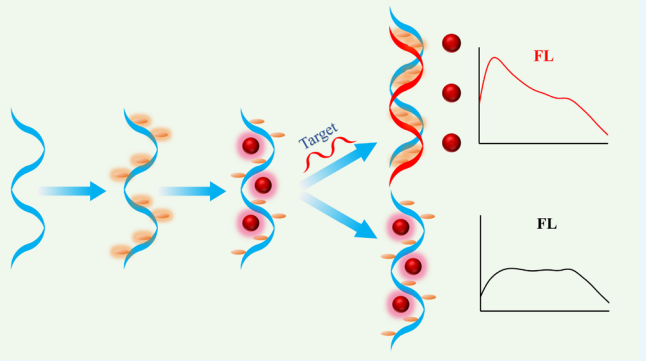

1. INTRODUCTION

The early diagnosis of cancer is of great significance to gain valuable time for the follow-up therapy. Traditional detection methods such as computed tomography, magnetic resonance imaging, endoscopy, and tissue biopsy play an important role in cancer diagnosis. However, the application of these traditional methods in early diagnosis is limited by their sensitivity and damage to tissues. In recent years, an emerging non-invasive diagnostic technology, liquid biopsy, is booming. Compared to traditional cancer diagnosis methods, liquid biopsy has merits in sensitivity, safety, prospectiveness, and subsequent treatment guidance.[1−3] The biomarkers of cancer liquid biopsy involve circulating tumor cells, exosomes, circulating tumor DNA, and RNA. Among them, miRNAs, a group of small noncoding single-stranded RNA, are considered to play key roles in the prediction of cancer progression.[4−6] Thus, it is attractive to develop liquid biopsy technologies toward cancer-specific miRNA to achieve the early cancer diagnosis.

So far, medical detection methods for miRNA such as Northern blot, quantitative real-time polymerase chain reaction, and microarray analysis have been used for disease diagnosis based on their high yield, good repeatability, and powerful anti-interference ability. Nevertheless, they have problems in low sensitivity and specificity, poor portability, and long detection period. A new hotspot in miRNA detection is the fusion of materials science and medicine.[7−9] The feasibility of this hotspot relies on the signal response of materials and the complementary base pairing between the probe molecule and the target miRNA. The signal response of materials is based on various types of principles such as fluorescence, surface-enhanced Raman spectroscopy, colorimetry, and electrochemistry.[10−13] Comparatively, the fluorescence method has received more attention due to its characteristics of high sensitivity and convenient analysis.[4,14] For instance, Chinnappan *et al.* reported the detection of breast cancer miRNA sequences based on the change in fluorescence intensity caused by the change in the distance

Received: October 21, 2021
Accepted: November 22, 2021
Published: November 30, 2021

https://doi.org/10.1021/acsomega.1c05901
ACS Omega 2021, 6, 34150−34159

between the fluorophore and the quencher that was triggered by the target miRNA.[15] This sensor was applied to detect the miRNA incorporated into the total RNA isolated from whole blood. In another work, Oudeng *et al.* proposed a one-step detection probe for *in situ* detection of the target miRNA in single live cancer cells based on the fluorescence switch of MoS_2 nanosheets.[16] The detection ability of this sensor to endogenous miRNA was demonstrated by using MCF-7 and HeLa cells. Although the aforementioned fluorescence-based sensors can detect miRNA, the reliability is affected by the background fluorescence and the stability of excitation light.[17,18] Therefore, attention should be focused on reducing or eliminating the interference of destabilizing factors to improve the reliability of the fluorescence method.

Recent studies have shown that ratiometric fluorescent sensors can determine the concentration of miRNA based on the fluorescence intensity ratio of different fluorophores, which is more reliable than the sensors that rely on a single fluorophore.[19−21] Ratiometric fluorescent sensors can overcome various factors that single wavelength-based detecting systems are susceptible to, such as the concentration change of sensors, drift of light source or detector, optical path length, and the complex sample or system environment. The change in fluorescence intensity ratio is based on the distance change between different fluorescent molecules caused by the conformational change of the fluorescent probe. To fabricate a ratiometric fluorescent sensor, several conditions for Forster resonance energy transfer (FRET) must be met between the fluorophores (donor and acceptor), that is, the fluorescence spectra are matched, the distance is in the range of 1−10 nm, and the dipole spatial orientation is consistent. The challenge of fabricating a ratiometric fluorescent biosensor lies in the matching of fluorescent donor−acceptor pairs. Fluorescent carbon dots (CDs), a class of typical fluorescent nanomaterials, show bright prospects in the fields of biological detection and imaging due to their adjustable fluorescence, high brightness and stability, low biological toxicity, excellent water solubility, and large Stokes shift.[22−24] Given these advantages, the construction of a CD-based ratiometric biosensor may be a feasible strategy for sensitive detection of miRNA. Acridine orange (AO) is a cationic nucleic acid fluorescent dye with a maximum emission wavelength of about 530 nm.[25] AO can be adsorbed on the phosphate side of single-stranded nucleic acids through charge attraction. In the presence of double-stranded nucleic acids, AO is inserted into the base pair gap through a strong π bond. A clever use of the binding state between AO and single/double-stranded nucleic acids has the possibility of fabricating a fluorescence detection system based on molecular surface properties. In addition, detection strategies that rely on an expensive duplex-specific nuclease enzyme are extremely costly. Hence, it is cost-effective to explore enzyme-free miRNA detection strategies.

Herein, a FRET system composed of CDs and AO is proposed to achieve the enzyme-free ratiometric fluorescence detection of miRNA. Reliable ratiometric fluorescence detection is realized by precisely regulating and utilizing the fluorescence property and surface charge of the component molecules. The physicochemical properties of the CDs and the fluorescence characteristics of AO were analyzed to demonstrate that they met the requirements for forming the FRET system. The identified colorectal cancer biomarker miRNA (miR-92a-3p) was used as the target to test the effectiveness of the ratiometric fluorescent biosensor.[26] The sensitivity and selectivity of the ratiometric fluorescent biosensor to miR-92a-3p were investigated. Furthermore, the reliability of the proposed ratiometric fluorescent biosensor was verified by measuring the concentration of miR-92a-3p in the serum sample.

2. EXPERIMENTAL SECTION

2.1. Materials and Apparatus. Citric acid ($C_6H_8O_7$, AR grade), formamide (CH_3NO, AR grade), acridine orange ($C_{17}H_{19}N_3$, biotechnology grade), tetraethyl orthosilicate ($C_8H_{20}O_4Si$, GC grade), ammonium hydroxide solution ($NH_3{\cdot}H_2O$, AR grade), triethylamine ($C_6H_{15}N$, AR grade), glutaric anhydride ($C_5H_6O_3$, 98%), sodium chloride (NaCl, AR grade), (3-aminopropyl)triethoxysilane ($C_9H_{23}NO_3Si$, 99%), *N*-(3-dimethylaminopropyl)-*N*′-ethylcarbodiimide hydrochloride ($C_8H_{17}N_3{\cdot}HCl$, 98.5%), and *N*-hydroxysuccinimide ($C_4H_5NO_3$, 99%) were purchased from Shanghai Macklin Biochemical Co., Ltd. Ethanol anhydrous (C_2H_6O, AR grade), methanol (CH_4O, AR grade), acetone (C_3H_6O, AR grade), and toluene (C_7H_8, AR grade) were purchased from Sinopharm Chemical Reagent Co., Ltd. The other reagents used were of AR grade without further purification, and ultrapure water was used in all experiments. The miR-92a-3p, DNA probe, amino-modified DNA (NH_2-DNA) probe, and unmatched targets were purchased from Shanghai Genepharma Co., Ltd. Their sequences are listed in Table S1 of the Supporting Information. The human serum was isolated from the healthy sample from the Second Hospital of Shandong University. The apparatus used are given in the Supporting Information.

2.2. Preparation of CDs. The CDs were prepared based on a previously reported work.[27] Typically, 10 mmol of citric acid was dissolved in 30 mL of formamide, transferred to a Teflon-lined reactor with a volume of 50 mL, and then reacted at 180 °C for 6 h. The reaction between citric acid and formamide is shown in Scheme 1. After the solution was cooled to room temperature, 100 mL of acetone was added and kept at −20 °C for 24 h to obtain CD precipitation. Then, the CD precipitate was washed several times with acetone and 10% methanol/acetone solution in turn and redispersed in 10 mL of methanol. The above solution was filtered with a membrane with a pore size of 0.22 μm to remove large particles, and acetone was added and centrifuged to obtain purified CDs. Finally, a CD powder was obtained by vacuum drying at 40 °C for 6 h.

Scheme 1. Chemical Reaction Formula for the Synthesis of CDs Using Citric Acid and Formamide as Raw Materials

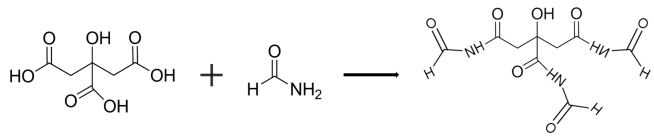

2.3. Preparation of Carboxyl-Modified SiO_2 Microspheres (COOH-SiO_2). *2.3.1. Preparation of SiO_2 Microspheres.* Five milliliters of tetraethyl orthosilicate was dispersed in 20 mL of absolute ethanol and stirred for 30 min to obtain solution A. Solution B was composed of 25 mL of ethanol, 10 mL of ultrapure water, and 5 mL of ammonia. Solution A was added dropwise to solution B under stirring and reacted at 40 °C for 6 h. The product was washed with

https://doi.org/10.1021/acsomega.1c05901
ACS Omega 2021, 6, 34150−34159

Scheme 2. Schematic Illustration of the Ratiometric Fluorescence System[a]

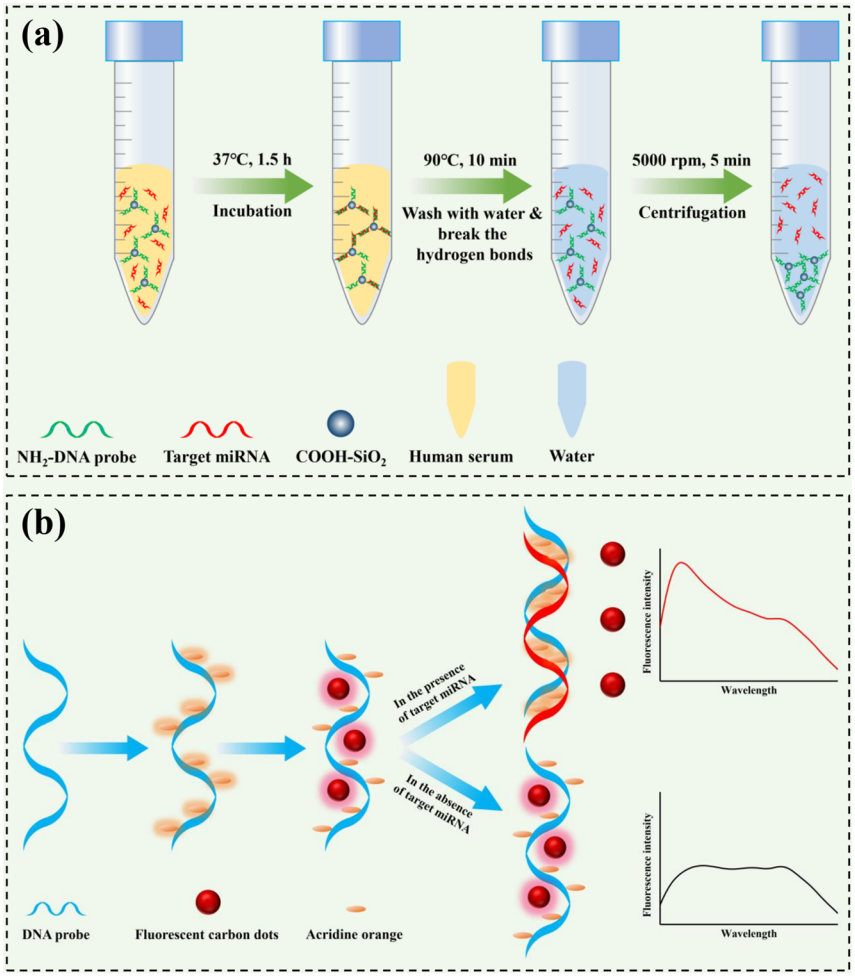

[a](a) Isolation of miRNA from serum by COOH-SiO_2. (b) Ratiometric fluorescence detection of miRNA.

ethanol and the SiO_2 microspheres were obtained by drying at 40 °C for 12 h.

2.3.2. Preparation of Silane-Modified SiO_2 Microspheres. SiO_2 microspheres (0.5 g) were ultrasonically dispersed in 20 mL of toluene, and then 1 mL of (3-aminopropyl)-triethoxysilane and 15 μL of triethylamine were added. The mixture was refluxed at 110 °C for 6 h. The product was washed with acetone and dried at 40 °C for 12 h to obtain silane-modified SiO_2 microspheres.

2.3.3. Carboxyl Modification of Silane-Modified SiO_2 Microspheres. Silane-modified SiO_2 microspheres (0.25 g) were ultrasonically dispersed in 10 mL of absolute ethanol, and then 10 mL of absolute ethanol solution containing 1 g of glutaric anhydride was added dropwise. The mixture was stirred at 37 °C for 5 h. The product was washed with 0.1 M NaCl solution and ethanol and dried at 40 °C for 12 h to obtain COOH-SiO_2.

2.4. Isolation of the Target miRNA from Serum. COOH-SiO_2 (0.2 mg), 0.01 mmol of *N*-(3-dimethylaminopropyl)-*N*′-ethylcarbodiimide hydrochloride, and 0.02 mmol of *N*-hydroxysuccinimide were ultrasonically dispersed in 200 μL of MES buffer solution (pH 5.5, 1 mM) and reacted at 25 °C for 15 min. Then, the dispersion was washed by centrifugation and the substrate was dispersed in 150 μL of PBS buffer (pH 7.4, 1 mM). Subsequently, 50 μL of NH_2-DNA probe (10 μM) was immediately added and reacted at 25 °C for 2 h. After that, the substrate was washed several times with ultrapure water. Next, the substrate was ultrasonically dispersed in 175 μL of ultrapure water and 25 μL of serum with a preset miR-92a-3p concentration of 10 μM and incubated at 37 °C for 1.5 h. The incubated product was washed several times with ultrapure water. Subsequently, 25 μL of ultrapure water was added to the incubation product and kept at 90 °C for 10 min. The concentration of miR-92a-3p in the supernatant after centrifugation was theoretically equal to that in the serum.

2.5. Fluorescence Detection of miRNA. First, 3 μL of DNA probe solution (1 μM) and 3 μL of target miRNA solution were added to 290 μL of ultrapure water and incubated at 37 °C for 1.5 h. Then, 2 μL of AO solution (11 μM) was added and kept for 10 min. Subsequently, 2 μL of CD solution (0.08 mg/mL) was added and kept for 20 min. Finally, the fluorescence spectra were collected by a fluorescence spectrophotometer under the following instrument settings: the excitation wavelength was 492 nm, the excitation slit and emission slit were both 10 nm, and the emission spectra were collected in the range of 512−675 nm. Each fluorescence intensity data point represents the average of three independent experiments.

https://doi.org/10.1021/acsomega.1c05901
ACS Omega 2021, 6, 34150−34159

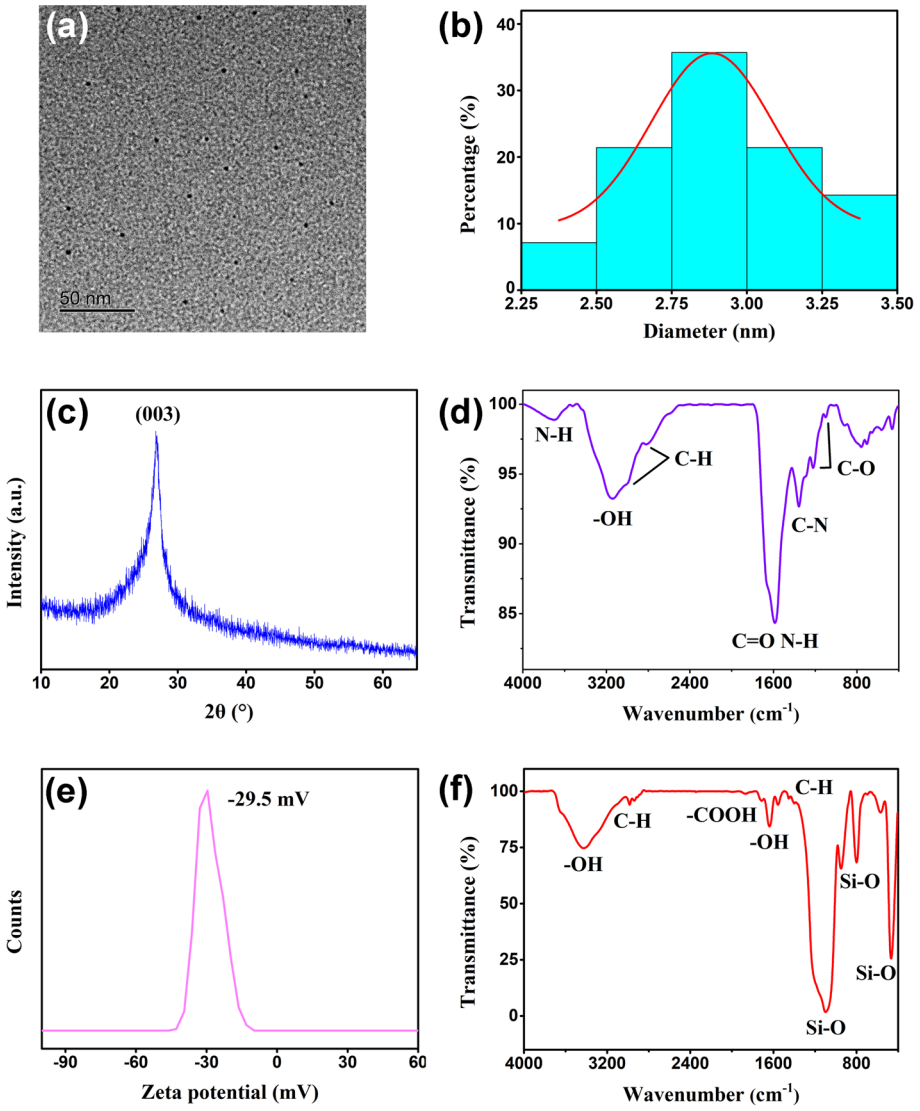

Figure 1. Characterization of CDs and COOH-SiO_2. (a) TEM image of CDs. (b) Size distribution of CDs calculated according to panel (a). (c) XRD pattern, (d) FTIR spectrum, and (e) zeta potential of CDs. (f) FTIR spectrum of COOH-SiO_2.

3. RESULTS AND DISCUSSION

3.1. Principle of the Ratiometric Fluorescent Biosensor. Before the detection, the target miRNA was isolated from the serum to avoid the interference of other nucleic acids on the fluorescence signal. The miRNA isolation process is shown in Scheme 2a. First, the NH_2-DNA probe modified on the surface of COOH-SiO_2 and the target miRNA in the serum were incubated at 37 °C for 1.5 h to form a complementary strand. Then, the serum was washed away with ultrapure water. Finally, the hydrogen bonds between the complementary strands were broken by maintaining the solution temperature at 90 °C for 10 min, and the NH_2-DNA probe-modified COOH-SiO_2 and miRNA were separated by centrifugation.

Scheme 2b depicts the detection principle of the ratiometric fluorescent biosensor. For nucleic acids, the phosphate side is negatively charged due to the ionization of hydrogen ions. When the cationic dye AO and CDs with negative surface charge are added to the DNA probe solution, AO is adsorbed on the phosphate side due to charge attraction, and CDs are adsorbed on the base side due to $\pi-\pi$ conjugation and hydrogen bonding.[28] In detail, the acridine ring nitrogen atom of acridine orange is combined with the phosphate oxygen ion of the probe through electrostatic attraction. The internal graphitization structure, carbonyl, hydroxyl, and amide of CDs are combined with the carbocyclic, amino, and carbonyl groups of the base through $\pi-\pi$ conjugation and hydrogen bonding. The close distance results in the FRET between AO and CDs. As a result, the fluorescence intensity of AO decreases, while the fluorescence of CDs increases. The adsorption of CDs on the base side of the DNA probe was verified by zeta potential. As shown in Figure S1 and Figure 1e, the presence of the DNA probe reduced the zeta potential due to the exposure of the phosphate of the DNA probe after adsorption. When the target miRNA is presented, the DNA probe and target miRNA form the complementary strand by complementary base pairing. In the case of double-stranded nucleic acids, the base is wrapped and the phosphate is exposed to exhibit a negative charge in aqueous solution. AO is inserted into the base pair gap of the complementary strand by the strong π bond, while the CDs are far away from the complementary strand due to the base being wrapped and charge repulsion. In this case, the decrease or disappearance of FRET leads to the recovery of the fluorescence of AO and the decrease of the fluorescence

https://doi.org/10.1021/acsomega.1c05901
ACS Omega 2021, 6, 34150−34159

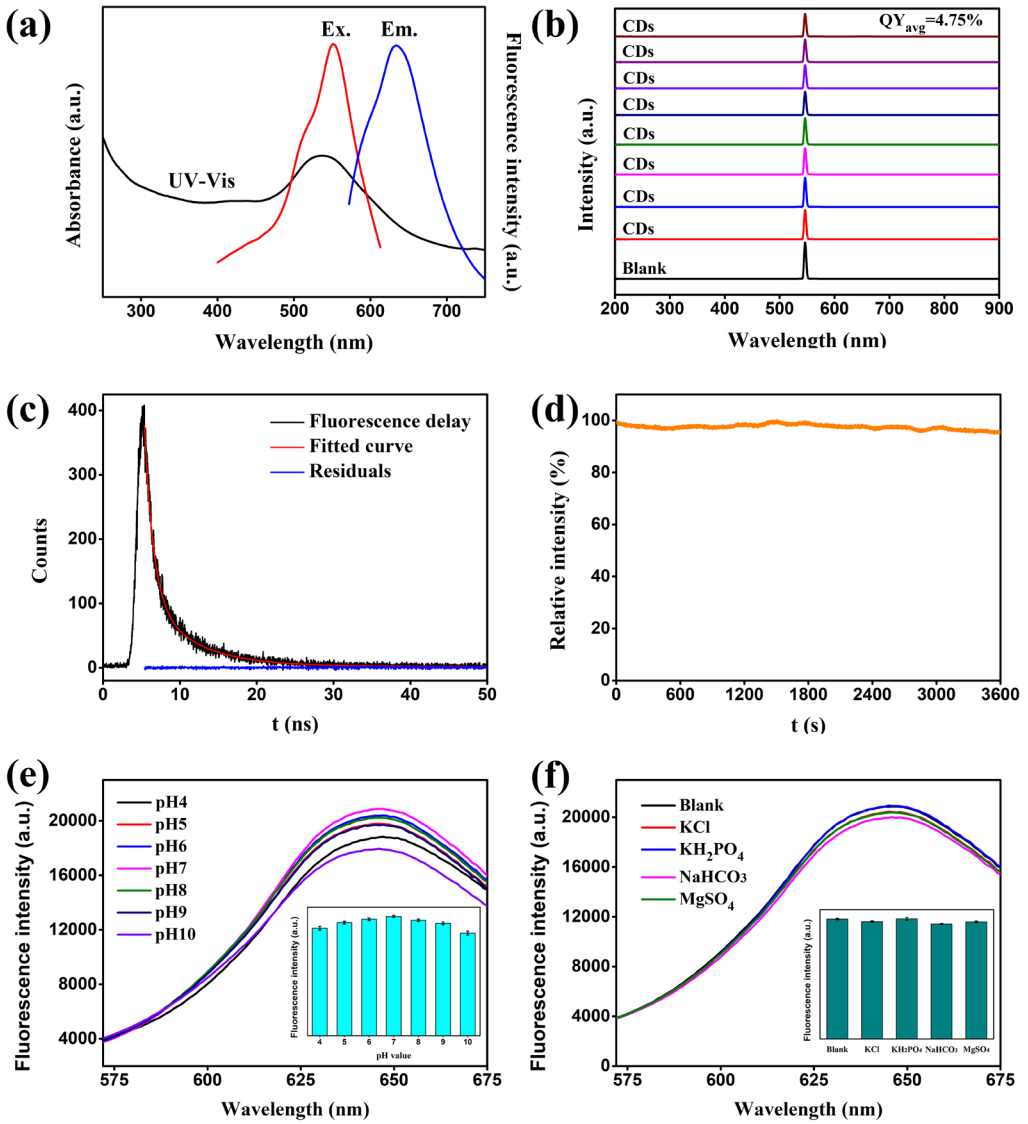

Figure 2. Fluorescence properties of CDs. (a) UV−Vis absorption spectrum and fluorescence excitation and emission spectra of CDs. (b) Absolute quantum efficiency and (c) fluorescence lifetime of CDs. (d) Fluorescence intensity of CDs under continuous irradiation for 1 h. (e) Influence of pH and (f) inorganic salt ions on the fluorescence intensity of CDs.

intensity of CDs. The AO/CD fluorescence intensity ratio is proportional to the concentration of the target miRNA.

3.2. Characterization of CDs and COOH-SiO$_2$. It can be seen from Figure 1a that CDs were monodispersed and uniform in size. The statistics from over 20 CDs showed that the size of CDs was in the range of 2.25−3.50 nm with an average size of 2.94 nm (Figure 1b). Figure 1c demonstrates that the CDs exhibited both graphitic and amorphous forms. The incomplete graphitization of CDs was also confirmed by the Raman spectrum in Figure S2. This is in line with the recognition that the synthesized carbon-based materials under solvothermal conditions mainly show an amorphous edge modified by functional groups and the graphitized core.[29,30] FTIR analysis was performed to determine the functional groups of CDs (Figure 1d). The broad absorption bands with peaks at 3695 and 3140 cm^{-1} indicated the existence of N−H and −OH bonds, respectively. The absorption peaks at 2998 and 2820 cm^{-1} were attributed to the stretching vibrations of methyl and methylene. The absorption band with a peak at 1584 cm^{-1} was attributed to the C═O stretching vibration and N−H bending vibration. The absorption peak at 1356 cm^{-1} was attributed to the C−N stretching vibration. The absorption peaks at 1219 and 1098 cm^{-1} were attributed to the C−O stretching vibration. The FTIR spectrum demonstrated that the carboxyl that was attributed to the precursor citric acid was not presented in CDs. This was because the carboxyl of citric acid and the amino of formamide underwent an amidation reaction under solvothermal conditions.[27] The surface charge of CDs in aqueous solution determines the attraction/repulsion property of CDs and nucleic acids. The zeta potential of −29.5 mV leads to the repulsion between CDs and double-stranded nucleic acids (Figure 1e). Moreover, the morphology and functional groups of COOH-SiO$_2$ were characterized. As shown in Figure S3, the monodispersed COOH-SiO$_2$ exhibited an average size of about 300 nm. In addition to Si−O and −OH, the absorption bands attributed to C−H and −COOH appeared in the FTIR spectrum of COOH-SiO$_2$, indicating that the carboxyl was successfully modified on SiO$_2$ (Figure 1f).[31]

https://doi.org/10.1021/acsomega.1c05901
ACS Omega 2021, 6, 34150−34159

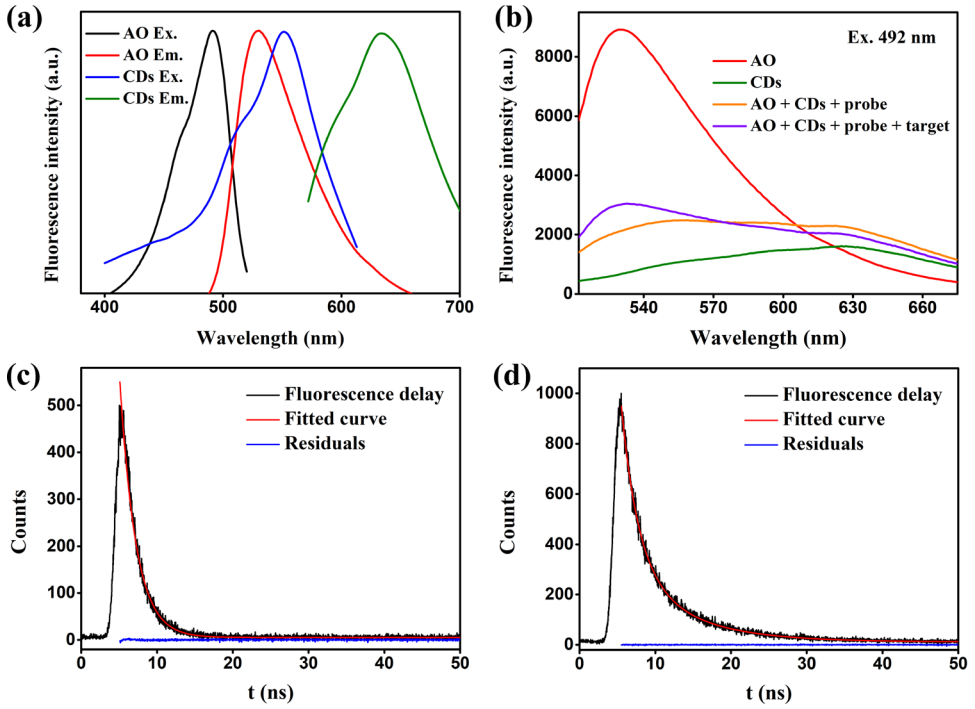

Figure 3. (a) Fluorescence excitation and emission spectra of AO and CDs. (b) Fluorescence spectra of AO, CDs, AO + CDs + DNA probe, and AO + CDs + DNA probe + target miRNA. Fluorescence lifetime of (c) AO and (d) AO + CDs.

3.3. Fluorescence Properties of CDs. The UV−Vis spectrum of CDs was measured to determine the electronic transition mechanism. The intense absorption band of CDs at $\lambda_{max} \approx 537$ nm could be attributed to the $n \rightarrow \pi^*$ transition of the π system (Figure 2a). In addition, the fluorescence excitation and emission peaks of CDs were identified as 551 and 634 nm, respectively. As shown in Figure 2b, the average absolute quantum efficiency of CDs in ultrapure water measured under the optimal excitation wavelength (551 nm) was 4.75%. To further understand the fluorescence properties of the CDs, the time-resolved fluorescence spectrum under excitation at 551 nm was measured, and an average lifetime of 4.46 ns was determined according to the fitting of the fluorescence decay curve (Figure 2c). The lifetime of nanosecond level means the singlet state nature of CD emission.[27] The fluorescence stability of CDs was measured by continuous irradiation at 551 nm for 1 h, and the fluorescence intensity curve is shown in Figure 2d. The fluorescence intensity of CDs fluctuated slightly under continuous light and maintained 99.24% of the initial value, which proved that CDs had excellent fluorescence stability. To further understand the stability of CDs, the effects of solution pH and inorganic salt ions on the fluorescence of CDs were measured. Figure 2e indicates that CDs showed the highest fluorescence intensity in neutral aqueous solution and that the increase in H^+ or OH^- concentration led to the decrease in fluorescence intensity. Figure 2f shows the fluorescence spectra of CDs in different inorganic salt solutions with a concentration of 1 mM. The fluorescence intensities of CDs in KCl, KH_2PO_4, $NaHCO_3$, and $MgSO_4$ solutions were 98, 100.2, 95.9, and 97.7% of that in ultrapure water, respectively. The inorganic salt ions have a slight effect on the fluorescence intensity of CDs. In addition, the long-term storage stability of the CD solution was also determined. As shown in Figure S4, the CD solution stored for 3 months kept a clear state without precipitation and its fluorescence intensity was 99.63% of the fresh one, proving that the CDs could be stored for a long term without affecting its fluorescence performance.

3.4. Feasibility of the Ratiometric Fluorescent Biosensor. Besides the distance change due to the charge interaction described in Sections 3.1 and 3.2, the fluorescence conditions that the FRET system should meet were also measured. As shown in Figure 3a, the maximum excitation wavelength of AO was 492 nm. Thus, the excitation wavelength of 492 nm was used in verifying the feasibility of the ratiometric fluorescent biosensor and the subsequent miRNA detection. There was a small overlap in the fluorescence excitation spectra of AO and CDs, and the fluorescence excitation peaks of CDs and AO were 60 nm apart. Hence, excitation under 492 nm would not result in significant fluorescence emission of CDs. On the other hand, there was a large proportion of overlap between the emission spectrum of AO and the excitation spectrum of CDs, which was beneficial to the FRET between AO and CDs.[32] The distance between the fluorescence peaks of CDs and AO was 104 nm, which made it easy to distinguish them in the miRNA detection.

The above analysis is confirmed by the fluorescence spectra in Figure 3b. In the AO + CDs + DNA probe system, the fluorescence intensity of AO decreased, while that of CDs increased compared to the individuals, indicating that the FRET occurred between AO and CDs. When the target miRNA was presented in the system, the fluorescence intensity of AO increased, while that of CDs decreased, indicating that the FRET was attenuated. Since FRET can shorten the fluorescence lifetime of the donor, the FRET was further verified by measuring the fluorescence lifetime of AO.[33] As shown in Figure 3c,d, the fluorescence lifetimes of AO in the absence and presence of CDs were 2.262 and 2.117 ns, respectively, which proved the occurrence of FRET. In short,

https://doi.org/10.1021/acsomega.1c05901
ACS Omega 2021, 6, 34150−34159

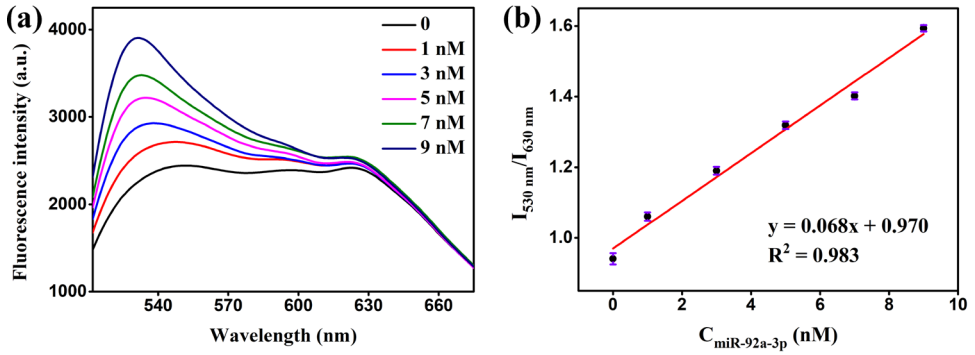

Figure 4. (a) Fluorescence spectra of the ratiometric fluorescent biosensor under different target miRNA concentrations. (b) Linear relationship between the AO/CD fluorescence intensity ratio and the target miRNA concentration.

the proposed ratiometric fluorescent biosensor could be used for the detection of miRNA.

3.5. Sensitivity of the Ratiometric Fluorescent Biosensor. The sensitivity of the ratiometric fluorescent biosensor was investigated by measuring the fluorescence spectra with different target miRNA concentrations. Figure 4a shows that the fluorescence intensity of AO increased as the concentration of the target miRNA increased from 0 to 9 nM. The slight change in the fluorescence intensity of CDs was attributable to the increase in the fluorescence intensity of AO, offsetting the decrease in the fluorescence intensity of CDs. As shown in Figure 4b, a highly fitted linear relationship (R^2 = 0.983) was presented between the AO/CDs fluorescence intensity ratio and the concentration of the target miRNA in the range of 0−9 nM, indicating that the concentration measurement of the ratiometric fluorescent biosensor was highly repeatable. The detection limit of the ratiometric fluorescent biosensor based on the 3σ method was 0.14 nM. Table 1 lists some representative works of detecting miRNA based on the FRET principle. In terms of detection limit, the sensitivity of our proposed enzyme-free ratiometric fluorescent biosensor is satisfactory.

Table 1. Representative Works of miRNA Detection Based on the FRET Principle

fluorophore	target	linear range (nM)	detection limit (nM)	ref.
FAM/TAMRA	miRNA-21	0−20	0.073	21
eosin Y	miRNA-21	0.2−20	0.098	34
2-aminopurine	MiRNA-21	0−400	0.5	35
UCNPs	miRNA-21	4−500	4	36
FAM	MiRNA-21	10−50		16
CuNPs	miRNA let-7a	0.5−100	0.2	37
AgNCs	miRNA-141	0−200	0.297	38
CdSe/ZnS QDs	miRNA	10−2000	4.2 ± 0.3	39
CDs/AO	miR-92a-3p	0−9	0.14	this work

3.6. Selectivity of the Ratiometric Fluorescent Biosensor. Selectivity is another important evaluation index of a sensor. The single-base mismatch target (SMT), two-base mismatch target (TMT), and noncomplementary target (miR-223-3p) were applied as control targets to evaluate the selectivity of the ratiometric fluorescent biosensor. Figure 5a shows the AO/CD fluorescence intensity ratio of the target miRNA and the mismatched miRNAs at a preset concentration of 5 nM. The concentrations of miR-223-3p, TMT, and SMT calculated according to the linear fitting curve were close to 0. They were much lower than the measured target miRNA concentration of 5.12 nM. Therefore, the proposed ratiometric fluorescent biosensor has high selectivity.

3.7. Detection of miRNA in Serum. The miRNA concentrations in serum were measured to verify the practicality of the proposed ratiometric fluorescent biosensor. Before the detection, the target miRNA was isolated from the serum by COOH-SiO_2 to avoid the interference of other nucleic acids. The modification of nucleic acids can increase the surface electronegativity of COOH-SiO_2 due to the negative surface charge of nucleic acids.[40] The zeta potentials of COOH-SiO_2, DNA probe-modified COOH-SiO_2, and target miRNA-conjugated COOH-SiO_2 are shown in Figure S5. The modification of the DNA probe and the conjugation of the target miRNA caused the increasing negative zeta potential of COOH-SiO_2 from −54.4 mV to −57.3 and −61.2 mV, respectively, indicating that COOH-SiO_2 captures the target miRNA. The effectiveness of the miRNA isolation by COOH-SiO_2 was tested by 10% nondenaturing polyacrylamide gel electrophoresis. As shown in Figure S6, the position and brightness of the electrophoretic bands of the isolated miRNA and the control were almost the same, indicating that the hybridization of the capture probes and miRNA was effectively initiated, and there was almost no loss in the isolation process. The serum miRNA concentrations of 1, 5, and 9 nM were preset. As shown in Figure 5b, the average recovery rates at the preset serum miRNA concentrations of 1, 5, and 9 nM were 95.19, 95.52, and 97.89%, respectively. The measured serum miRNA concentrations using the ratiometric fluorescent biosensor were close to the preset values. Thus, the ratiometric fluorescent biosensor can accurately detect serum miRNA. In addition, the measured values of serum miRNA at different concentrations were slightly lower than the preset values, which was probably due to the loss or degradation of miRNA in the isolation procedure.

4. CONCLUSIONS

In this work, a ratiometric fluorescent biosensor composed of carbon dots and acridine orange was fabricated based on the FRET principle, and its performance was tested with colorectal cancer-specific miRNA miR-92a-3p as the target. The charge properties of the DNA probe, target miRNA, CDs, and AO and the fluorescence characteristics of CDs and AO are the

https://doi.org/10.1021/acsomega.1c05901
ACS Omega 2021, 6, 34150−34159

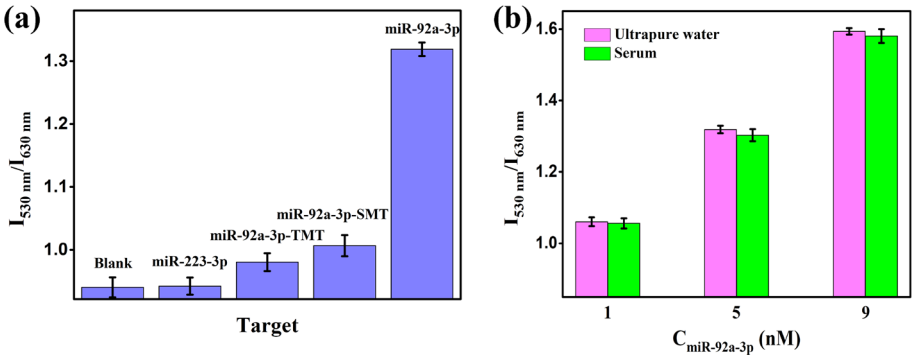

Figure 5. (a) Selectivity of the ratiometric fluorescent biosensor toward miR-92a-3p and mismatched miRNAs at a preset concentration of 5 nM. (b) Comparison of the measurement of miRNA concentration in ultrapure water and isolated from serum.

factors that ensure the feasibility of the ratiometric fluorescent biosensor. The ratiometric fluorescent biosensor showed a low detection limit of 0.14 nM for the target miRNA. Control experiments demonstrated that the ratiometric fluorescent biosensor had high selectivity to distinguish target miRNA from other miRNAs. In terms of reliability, the designed isolation−detection strategy can accurately reflect the concentration of serum miRNA. Furthermore, the proposed ratiometric fluorescent biosensor can also been applied to detect other miRNA biomarkers in theory by simply replacing the DNA probe according to the target miRNA sequence. Our research contributes to designing an "all-in-one" testing kit in the future to realize accurate miRNA analysis in clinical practice.

■ ASSOCIATED CONTENT

Supporting Information

The Supporting Information is available free of charge at https://pubs.acs.org/doi/10.1021/acsomega.1c05901.

Apparatus; sequences of nucleic acids; characterizations (zeta potential, Raman spectrum, TEM image, fluorescence spectra, and nondenaturing polyacrylamide gel electrophoresis (Figures S1−S6)) (PDF)

■ AUTHOR INFORMATION

Corresponding Authors

Lutao Du − *Department of Clinical Laboratory, The Second Hospital, Cheeloo College of Medicine, Shandong University, Jinan 250033, China*; Email: lutaodu@sdu.edu.cn

Yanyan Jiang − *Key Laboratory for Liquid−Solid Structural Evolution and Processing of Materials, Ministry of Education, Shandong University, Jinan 250061, China; Shenzhen Research Institute of Shandong University, Shenzhen 518057, China; Suzhou Institute of Shandong University, Suzhou 215123, China;* orcid.org/0000-0002-7866-4689; Email: yanyan.jiang@sdu.edu.cn

Authors

Zhiwei Sun − *Key Laboratory for Liquid−Solid Structural Evolution and Processing of Materials, Ministry of Education, Shandong University, Jinan 250061, China; Shenzhen Research Institute of Shandong University, Shenzhen 518057, China*

Yao Tong − *Department of Clinical Laboratory, The Second Hospital, Cheeloo College of Medicine, Shandong University, Jinan 250033, China*

Xiaoyu Zhou − *Key Laboratory for Liquid−Solid Structural Evolution and Processing of Materials, Ministry of Education, Shandong University, Jinan 250061, China*

Juan Li − *Department of Clinical Laboratory, The Second Hospital, Cheeloo College of Medicine, Shandong University, Jinan 250033, China*

Li Zhao − *Key Laboratory for Liquid−Solid Structural Evolution and Processing of Materials, Ministry of Education, Shandong University, Jinan 250061, China*

Hui Li − *Key Laboratory for Liquid−Solid Structural Evolution and Processing of Materials, Ministry of Education, Shandong University, Jinan 250061, China;* orcid.org/0000-0002-1457-8650

Chuanxin Wang − *Department of Clinical Laboratory, The Second Hospital, Cheeloo College of Medicine, Shandong University, Jinan 250033, China; Shandong Engineering & Technology Research Center for Tumor Marker Detection, Jinan 250033, China; Shandong Provincial Clinical Medicine Research Center for Clinical Laboratory, Jinan 250033, China;* orcid.org/0000-0002-3796-6293

Complete contact information is available at: https://pubs.acs.org/10.1021/acsomega.1c05901

Author Contributions

[▽]Z.S. and Y.T. contributed equally to this work.

Notes

The authors declare no competing financial interest.

■ ACKNOWLEDGMENTS

The authors acknowledge financial support from the Shenzhen Fundamental Research Program (grant no. JCYJ20190807092803583), the Guangdong Basic and Applied Basic Research Foundation (grant no. 2019A1515110846), and the National Natural Science Foundation of China (grant no. U1806219). The special funding also supports this work in the Project of the Qilu Young Scholar Program of Shandong University.

■ REFERENCES

(1) Fu, Y.; Zhang, Y.; Khoo, B. L. Liquid Biopsy Technologies for Hematological Diseases. *Med. Res. Rev.* **2021**, *41*, 246−274.

(2) Luo, W.; Rao, M.; Qu, J.; Luo, D. Applications of Liquid Biopsy in Lung Cancer-Diagnosis, Prognosis Prediction, and Disease Monitoring. *Am. J. Transl. Res.* **2018**, *10*, 3911−3923.

(3) Liu, Y.; Fan, Z.; Zhou, Y.; Lin, J.; Yang, Y.; Yan, L.; Li, Y.; Jiang, L.; Yang, F.; Hu, Q.; Yu, J.; Chen, L.; Liao, Y. Self-Circulating

Electrochemiluminescence Chip for Sensitive Detection of Circulating Tumour Nucleic Acids in Blood. *Sens. Actuators, B* **2019**, *301*, 127088.
(4) Chen, N.; Li, J.; Feng, X.; Yang, Y.; Zhu, L.; Chen, X.; Liu, X.; Li, Y.; Wang, C.; Xia, L. Label-Free and Self-Assembled Fluorescent DNA Nanopompom for Determination of Mirna-21. *Microchim. Acta* **2020**, *187*, 432.
(5) Chu, Y. J.; Gao, Y. K.; Tang, W.; Qiang, L.; Han, Y. K.; Gao, J. W.; Zhang, Y.; Liu, H.; Han, L. Attomolar-Level Ultrasensitive and Multiplex Microrna Detection Enabled by a Nanomaterial Locally Assembled Microfluidic Biochip for Cancer Diagnosis. *Anal. Chem.* **2021**, *93*, 5129−5136.
(6) Babayan, A.; Pantel, K. Advances in Liquid Biopsy Approaches for Early Detection and Monitoring of Cancer. *Genome Med.* **2018**, *10*, 21.
(7) Tang, H.; Zhu, J.; Wang, D.; Li, Y. Dual-Signal Amplification Strategy for Mirna Sensing with High Sensitivity and Selectivity by Use of Single Au Nanowire Electrodes. *Biosens. Bioelectron.* **2019**, *131*, 88−94.
(8) Qi, Y.; Lu, X.; Feng, Q.; Fan, W.; Liu, C.; Li, Z. An Enzyme-Free Microrna Assay Based on Fluorescence Counting of Click Chemical Ligation-Illuminated Magnetic Nanoparticles with Total Internal Reflection Fluorescence Microscopy. *ACS Sens.* **2018**, *3*, 2667−2674.
(9) Al Mubarak, Z. H.; Premaratne, G.; Dharmaratne, A.; Mohammadparast, F.; Andiappan, M.; Krishnan, S. Plasmonic Nucleotide Hybridization Chip for Attomolar Detection: Localized Gold and Tagged Core/Shell Nanomaterials. *Lab Chip* **2020**, *20*, 717−721.
(10) Li, Y.; Yu, C.; Zhao, C.; Ren, C.; Zhang, X. Catalytic Hairpin Assembly Induced Dual Signal Enhancement for Rapid Detection of Mirna Using Fluorescence Light-up Silver Nanocluster. *Anal. Chim. Acta* **2019**, *1084*, 93−98.
(11) Hu, Y.; Wu, C.; Huang, S.; Luo, X.; Yuan, R.; Yang, X. A Novel Sers Substrate with High Reusability for Sensitive Detection of Mirna 21. *Talanta* **2021**, *228*, 122240.
(12) Shuying, L.; Rui, L.; Minmin, D.; Liyan, Z.; Yao, J.; Lijun, C.; Wei, Q.; Hua, W. High-Throughput, Selective, and Sensitive Colorimetry for Free Micrornas in Blood Via Exonuclease I Digestion and Hemin-G-Quadruplex Catalysis Reactions Based on a Ldquoself-Cleaningrdquo Functionalized Microarray. *Sens. Actuators, B* **2016**, *222*, 198−204.
(13) Liu, P.; Qian, X.; Li, X.; Fan, L.; Li, X.; Cui, D.; Yan, Y. Enzyme-Free Electrochemical Biosensor Based on Localized DNA Cascade Displacement Reaction and Versatile DNA Nanosheets for Ultrasensitive Detection of Exosomal Microrna. *ACS Appl. Mater. Interfaces* **2020**, *12*, 45648−45656.
(14) Li, X.; Huang, N.; Zhang, L.; Zhao, J.; Zhao, S. A T7 Exonuclease Assisted Dual-Cycle Signal Amplification Assay of Mirna Using Nanospheres-Enhanced Fluorescence Polarization. *Talanta* **2019**, *202*, 297−302.
(15) Chinnappan, R.; Mohammed, R.; Yaqinuddin, A.; Abu-Salah, K.; Zourob, M. Highly Sensitive Multiplex Detection of Microrna by Competitive DNA Strand Displacement Fluorescence Assay. *Talanta* **2019**, *200*, 487−493.
(16) Oudeng, G.; Au, M. T.; Shi, J. Y.; Wen, C. Y.; Yang, M. One-Step in Situ Detection of Mirna-21 Expression in Single Cancer Cells Based on Biofunctionalized MoS_2 Nanosheets. *ACS Appl. Mater. Interfaces* **2018**, *10*, 350−360.
(17) Ding, L.; Liu, H.; Zhang, L.; Li, L.; Yu, J. Label-Free Detection of Microrna Based on the Fluorescence Quenching of Silicon Nanoparticles Induced by Catalyzed Hairpin Assembly Coupled with Hybridization Chain Reaction. *Sens. Actuators, B* **2018**, *254*, 370−376.
(18) Li, C.; Xue, C.; Wang, J.; Luo, M.; Shen, Z.; Wu, Z.-S. Oriented Tetrahedron-Mediated Protection of Catalytic DNA Molecular-Scale Detector against in Vivo Degradation for Intracellular Mirna Detection. *Anal. Chem.* **2019**, *91*, 11529−11536.
(19) Liu, Y.; Shen, T.; Li, J.; Gong, H.; Chen, C.; Chen, X.; Cai, C. Ratiometric Fluorescence Sensor for the Microrna Determination by Catalyzed Hairpin Assembly. *ACS Sens.* **2017**, *2*, 1430−1434.
(20) Chen, X.; Xu, K.; Li, J.; Yang, M.; Li, X.; Chen, Q.; Lu, C.; Yang, H. Switch-Conversional Ratiometric Fluorescence Biosensor for Mirna Detection. *Biosens. Bioelectron.* **2020**, *155*, 112104.
(21) Wang, S.; Wang, L.; Xu, X.; Li, X.; Jiang, W. MnO_2 Nanosheet-Mediated Ratiometric Fluorescence Biosensor for Microrna Detection and Imaging in Living Cells. *Anal. Chim. Acta* **2019**, *1063*, 152−158.
(22) Liu, H. C.; Ding, J.; Zhang, K.; Ding, L. Construction of Biomass Carbon Dots Based Fluorescence Sensors and Their Applications in Chemical and Biological Analysis. *TrAC, Trends Anal. Chem.* **2019**, *118*, 315−337.
(23) Huang, J.; Li, F.; Guo, R.; Chen, Y.; Wang, Z.; Zhao, C.; Zheng, Y.; Weng, S.; Lin, X. A Signal-on Ratiometric Fluorometric Heparin Assay Based on the Direct Interaction between Amino-Modified Carbon Dots and DNA. *Microchim. Acta* **2018**, *185*, 260.
(24) Tian, M.; Liu, Y.; Wang, Y.; Zhang, Y. Yellow-Emitting Carbon Dots for Selective Detecting 4-Np in Aqueous Media and Living Biological Imaging. *Spectrochim. Acta, Part A* **2019**, *220*, 117117.
(25) Doynikova, A. N.; Vekshin, N. L. Detection of RNA Hydrolysis with Binase by Acridine Orange Fluorescence. *Appl. Biochem. Microbiol.* **2019**, *55*, 518−523.
(26) Zheng, G.; Du, L.; Yang, X.; Zhang, X.; Wang, L.; Yang, Y.; Li, J.; Wang, C. Serum Microrna Panel as Biomarkers for Early Diagnosis of Colorectal Adenocarcinoma. *Br. J. Cancer* **2014**, *111*, 1985−1992.
(27) Sun, S.; Zhang, L.; Jiang, K.; Wu, A.; Lin, H. Toward High-Efficient Red Emissive Carbon Dots: Facile Preparation, Unique Properties, and Applications as Multifunctional Theranostic Agents. *Chem. Mater.* **2016**, *28*, 8659−8668.
(28) Wang, Y.; Gao, D.; Zhang, P.; Gong, P.; Chen, C.; Gao, G.; Cai, L. A near Infrared Fluorescence Resonance Energy Transfer Based Aptamer Biosensor for Insulin Detection in Human Plasma. *Chem. Commun.* **2014**, *50*, 811−813.
(29) Gao, W.; Zhou, Y.; Xu, C.; Guo, M.; Qi, Z.; Peng, X.; Gao, B. Bright Hydrophilic and Organophilic Fluorescence Carbon Dots: One-Pot Fabrication and Multi-Functional Applications at Visualized Au^{3+} Detection in Cell and White Light-Emitting Devices. *Sens. Actuators, B* **2019**, *281*, 905−911.
(30) Yao, D.; Liang, A.; Jiang, Z. A Fluorometric Clenbuterol Immunoassay Using Sulfur and Nitrogen Doped Carbon Quantum Dots. *Microchim. Acta* **2019**, *186*, 323.
(31) Zhang, C.; Li, X.; Jiang, Z.; Zhang, Y.; Wen, T.; Fang, M.; Tan, X.; Alsaedi, A.; Hayat, T.; Wang, X. Selective Immobilization of Highly Valent Radionuclides by Carboxyl Functionalized Mesoporous Silica Microspheres: Batch, Xps, and Exafs Analyses. *ACS Sustainable Chem. Eng.* **2018**, *6*, 15644−15652.
(32) Yang, K.; Zhao, J.; Zhang, L.; Liu, R.; Liang, H.; Zhao, S. In Situ Ratiometric Fluorescence Imaging for Tracking Targeted Delivery and Release of Anticancer Drug in Living Tumor Cells. *ACS Appl. Bio Mater.* **2019**, *2*, 4687−4692.
(33) Inamdar, S. R.; Mulimani, B. G.; Savadatti, M. I.; Sapre, A. V.; Mukherjee, T. Energy Transfer Mechanisms in Laser Dye Mixtures. *Spectrosc. Lett.* **2002**, *35*, 293−307.
(34) Li, S.; He, K.; Liao, R.; Chen, C.; Chen, X.; Cai, C. An Interference-Free and Label-Free Sandwich-Type Magnetic Silicon Microsphere-Rgo-Based Probe for Fluorescence Detection of Microrna. *Talanta* **2017**, *174*, 679−683.
(35) Ma, C.; Liu, H.; Wu, K.; Chen, M.; Zheng, L.; Wang, J. An Exonuclease I-Based Quencher-Free Fluorescent Method Using DNA Hairpin Probes for Rapid Detection of Microrna. *Sensors* **2017**, *17*, 760.
(36) Zuo, C.; Guo, Y.; Li, J.; Peng, Z.; Bai, S.; Yang, S.; Wang, D.; Chen, H.; Xie, G. A Nanoprobe for Fluorescent Monitoring of Microrna and Targeted Delivery of Drugs. *RSC Adv.* **2021**, *11*, 8871−8878.
(37) Ma, Q.; Li, S. F. Y. Enzyme- and Label-Free Fluorescence Microrna Biosensor Based on the Distance-Dependent Photoinduced Electron Transfer of DNA/Cu Nanoparticles. *Microchem. J.* **2021**, *160*, 105646.
(38) Kim, H.; Kang, S.; Park, K. S.; Park, H. G. Enzyme-Free and Label-Free Mirna Detection Based on Target-Triggered Catalytic

https://doi.org/10.1021/acsomega.1c05901
ACS Omega 2021, 6, 34150−34159

Hairpin Assembly and Fluorescence Enhancement of DNA-Silver Nanoclusters. *Sens. Actuators, B* **2018**, *260*, 140−145.
(39) Bian, F.; Sun, L.; Cai, L.; Wang, Y.; Zhao, Y.; Wang, S.; Zhou, M. Molybdenum Disulfide-Integrated Photonic Barcodes for Tumor Markers Screening. *Biosens. Bioelectron.* **2019**, *133*, 199−204.
(40) Shi, Y.; Zhang, H.; Yue, Z.; Zhang, Z.; Teng, K.-S.; Li, M.; Yi, C.; Yang, M. Coupling Gold Nanoparticles to Silica Nanoparticles through Disulfide Bonds for Glutathione Detection. *Nanotechnology* **2013**, *24*, 375501.

https://doi.org/10.1021/acsomega.1c05901
ACS Omega 2021, 6, 34150−34159